MAGNETIC HARDENING OF EXCHANGE SPRING MULTILAYERS

T. SCHREFL, H. FORSTER, J. FIDLER, R. DITTRICH, D. SUESS, W. SCHOLZ
Solid State Physics, Vienna University of Technology, Wiedner Haupstr. 8-10/138, A-1040 Vienna, Austria

Abstract. Nanostructured permanent magnets have great potential for MEMS application, since it is possible to tailor their magnetic properties according to the specific requirements. In addition, hard magnetic / soft magnetic bilayers are excellent model systems to study fundamental magnetization processes both experimentally and numerically. The hysteresis properties of epitaxial SmCo/Co and SmCo/Fe bilayers are calculated by the solution of the Landau-Lifshitz Gilbert equation. The thin film grain structure is taken into account using appropriate finite element techniques. The J(H) curve shows the typical exchange spring behavior for a 10 nm Co-Sm / 10 nm Fe bilayer. However, the reversible rotations of the magnetization for low external field deteriorate the maximum energy density product. Straight B(H) curves are obtained only for a Fe layer thickness of 5 nm. The energy density products are 390 kJ/m^3 for 10 nm Co-Sm / 10 nm Fe, 405 kJ/m^3 for 10 nm Co-Sm / 5 nm Fe, and 644 kJ/m^3 for 2.5 nm Co-Sm / 5 nm Fe. If the soft magnetic layer is sufficiently small exchange interactions keep the magnetization aligned even in strong opposing fields. Magnetization reversal starts with the reversible rotation of the soft layer magnetization. Initially, the magnetization rotates in opposite directions in different regions of the film. The reversible rotations penetrate substantially into the hard layer. Magnetization angles up to 30 degrees with respect to the easy axis are found in a depth of 1.5 nm. If the expense of exchange energy becomes to large a reversed domain nucleates and expands in the hard layer.

1. Introduction

Understanding magnetization reversal is a fundamental issue in permanent magnets. The optimization of the magnetic properties requires a basic knowlegde of the interplay between magnetization reversal and nanoscale structural features. Micromagnetic simulations [9,7,27] provide the essential mechanisms that govern the magnetic properties of nanostructured magnets. Magnetic nanostructures composed of magnetically soft and hard phases show interesting properties since it is possible to increase the remanence due to the high saturation polarization of the soft phase. If both phases are sufficiently exchange coupled nanocomposite magnets show a reasonable high coercive field. Recent examples of nano-dispersed composites are bulk $Fe_3B/Nd_2Fe_{14}B$ magnets produced by rapid quenching and subsequent annealing, or by mechanically alloying [3,31]. The measured energy density products are comparable with those of isotropic, single phase magnets. In addition, nanocomposite may be cheaper than corresponding single phase magnets, owing to the lower rare-earth content.

Basic limits of bulk nanocomposite magnets arise from microstructural complexities that make it often difficult to optimize the magnetic properties. Thin film growth techniques, however, permit the preparation of artificial nano-disperse magnetic structures. Magnetron sputtering techniques enable to control the microstructure, the crystallographic orientation, and the magnetic anisotropy of multilayer hard magnetic / soft magnetic structures [10,13,15]. The saturation polarization and the stability of the soft magnetic phase against magnetization reversal determine the maximum achievable energy density product. The maximum possible energy density product is

$$(BH)_{\max} = \frac{J_s^2}{4\mu_0}, \tag{1}$$

provided that

$$|H_N| \geq \frac{J_s}{2\mu_0}, \tag{2}$$

where H_N is the nucleation field of the soft phase. If the external field reaches H_N the soft magnetic phase starts to reverse. Layered hard magnetic / soft magnetic structures have great potential for high energy density permanent magnets [28]. The high energy saturation polarization of the soft phase will increase J_s and in turn enable a high $(BH)_{\max}$ according to (1). A high magnetocrystal-

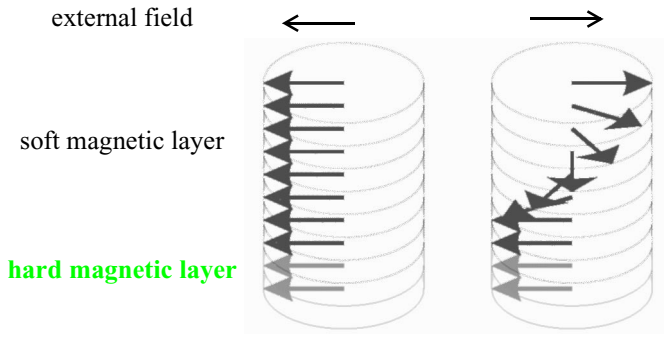

Fig. 1: The magnetization twist in an exchange spring bilayer. An reversed field larger than the absolute value of the nucleation field starts induces a gradually rotating magnetization within the soft layer.

line anisotropy of the hard phase is a prerequisite for the stabilization of the soft magnetic phase and in turn helps to fulfill equation (2). The saturation polarization J_s can be controlled by the intrinsic magnetic properties of the soft magnetic phase and the volume fraction of the soft magnetic phase. However, increasing the soft magnetic layer thickness, t_{soft}, will lead to a decrease of the nucleation field. According to Goto and co-workers [11] the nucleation field is

$$|H_N| = \frac{\pi^2 \mu_0 A_{soft}}{2 J_{s,soft} t_{soft}^2} \tag{3}$$

assuming an infinitely rigid hard layer. J_s and t_{soft} are interrelated in layered hard magnetic / soft magnetic structures. In order to optimize the energy density product it is required to increase both J_s and H_N. Thus it is necessary to identify the factors that initiate magnetization reversal in the soft phase, in order to realize the full potential of the exchange hardening principle.

Hard magnetic / soft magnetic multilayers have great potential for MEMS application [16], since it is possible to tailor their magnetic properties according to the specific requirements. For example, hard magnetic materials with a high remanent polarization can be used in bi-directional microactuators [5]. Another interesting feature of hard magnetic / soft magnetic multilayers with great potential for use in magnetoelectronic devices is the formation of confined domain walls. The magnetic polarization of the soft magnetic phase rotates reversibly out of its easy direction, which is parallel to the anisotropy direction of the adjacent hard phase, if a sufficiently large inverse magnetic field is applied. Within the soft magnetic phase the magnetization shows a twist with gradually rotating magnetization. The rotation angle increases with increasing distance from the hard phase, as schematically shown in Fig. 1. The magnetization forms a Bloch wall like structure and will rotate back in alignment with the hard phase when the applied field is reduced. This exchange spring behavior was originally proposed by Kneller and Hawig [17]. The magnetoresistance originating from the partial wall structure may be used in sensors or magneto-electronic devices [22].

Besides their possible applications layered hard magnetic, soft magnetic structures are excellent model systems to study fundamental magnetization processes. The growth and movement of domains walls and the reorientation of the moment direction near the interfaces are the characteristic features of exchange coupled systems. Prominent examples of exchange coupled systems are exchange-biased systems of ferromagnets and antiferromagnets [23] and exchange spring systems of soft and hard ferromagnets [10,13,15]. A deeper understanding of the magnetization processes in exchange coupled structures is beneficial for the improvement of current permanent magnets and

the development of new magnetic devices. Magnetization processes at hard magnetic / soft magnetic interfaces play a dominant role in the following application areas:

- The spin-dependent transport which is essential for application in spin electronic devices significantly depends on the magnetization structure near interfaces [21].
- The nucleation of reversed domains in hard magnetic grains touching a soft magnetic inclusions is the key element that limits the energy density product of sintered high performance magnets [6].
- Domain wall pinning on thin phases with a higher magnetocrystalline anisotropy than that in the adjacent regions is the coercivity mechanism of Sm_2Co_{17} based magnets for high temperature applications [12,18].
- Coercivity, remanence, and loop shape of low cost nanocomposite magnets depend on the magnetic properties and the arrangement of the magnetization near the hard magnetic /soft magnetic interface [14].
- The tailoring of the magnetic properties of high energy density hard magnetic / soft magnetic multilayers [10] requires a detailed understanding of the exchange hardening mechanism.

In this work we apply finite element micromagnetic simulations [4] to explore the basic features of SmCo based hard magnetic / soft magnetic bilayers. Section 2 of the paper introduces the numerical techniques and the finite element model of the investigated bilayer structures. Section 3 presents the magnetic properties calculated for SmCo thin film magnets. Section 4 and section 5 treat exchange hardening in SmCo / Co bilayers and SmCo / Fe bilayers. Section 6 summarizes the results and discusses the structural features required for high energy density product multilayer systems.

2. Finite element models

Epitaxial SmCo films grown by magnetron sputtering onto Cr-buffered MgO substrates show a granular structure with a grain size of about 30 nm [2]. In the case of MgO(100) substrates the $(11\bar{2}0)$-oriented SmCo shows a bicrystal structure. The c-axes of the grains lie in plane and are normal or perpendicular to each other. The grains of $(1\bar{1}00)$-oriented SmCo, grown on MgO(110) substrates, have in-plane c-axes which are parallel to each other, resulting in a uniaxial structure. We numerically calculated the hysteresis properties of $(11\bar{2}0)$-oriented SmCo and $(1\bar{1}00)$-oriented SmCo thin films, and of bilayers composed of a uniaxial SmCo film using Co or α-Fe as soft magnetic layer.

First a granular structure is calculated using a Voronoi construction [26]. Then the grains are further subdivided into tetrahedral finite elements. In order to resolve the relevant magnetization processes, the mesh size has to be sufficiently smaller than the domain wall width in the hard phase and has to be equal to the exchange length in the soft phase. To reduce the computational effort we reduce the lateral size of the film to 5 x 5 grains with a diameter of 30 nm. The total number of finite elements reaches 210 000 for the 10 nm thick SmCo film and 350 000 for the bilayer structures. We derive a system of exchange and magnetostatically coupled magnetic moments, assigning a magnetic moment to each node of the finite element mesh [30]. For each magnetic moment the Landau-Lifshitz Gilbert (LLG) equation [20] is solved. Owing to the exhange and the magnetostatic interactions between the magnetic moments, a system of coupled nonlinear differential equations has to be solved. A preconditioned, backward differentiation time integration scheme proved to be highly efficient to solve the dynamic micromagnetic equations of irregular magnetic structures [30]. Initially the magnetic system is saturated parallel to the applied field direction. Then the

LLG equation is integrated until equilibrium for decreasing applied field. Thus the quasi-static demagnetization curve can be obtained numerically. The magnetostatic interactions are calculated using a hybrid finite element / boundary element method [8]. A hierarchical multi-level method [1] is used to accelerate the boundary element method and to avoid the storage of the fully populated boundary element matrix.

High resolution transmission electron microscopy studies [2] show that the SmCo film consists of a mixture of $SmCo_3$, Sm_2Co_7, and $SmCo_5$ polytypoids. We randomly varied the magnetocrystalline anisotropy constant in the hard magnetic phase assuming 50 volume percent $SmCo_5$, in order to account for this mixture of phases. Table 1 summarizes the intrinsic magnetic properties used for the calculations.

Table 1: Intrinsic magnetic properties used for the calculations. For α-Fe zero magnetocrystalline anisotropy was assumed in the calculations.

	K_1 (MJ/m^3)	J_s (T)	A (pJ/m)	ref.
$SmCo_5$	17	1.07	8.6	[19,29]
Sm_2Co_7, $SmCo_3$	12	1.07	8.6	
Co	0.45	1.76	13	[32]
α-Fe	0	2.15	25	[17]

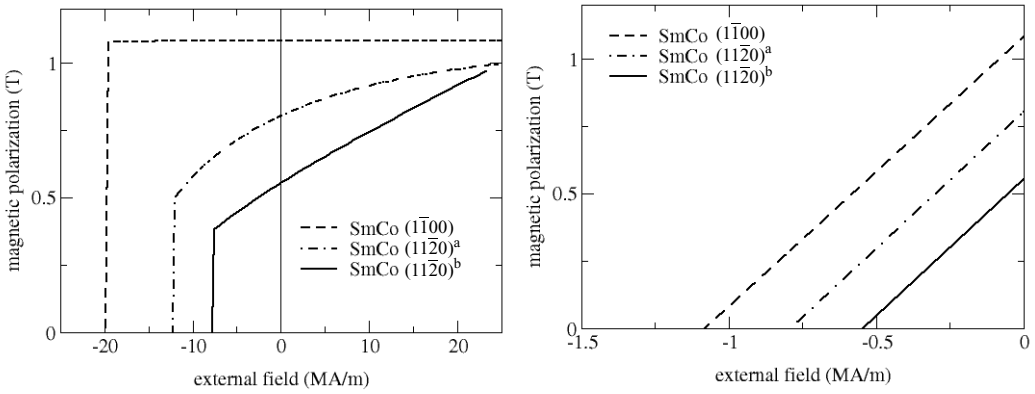

Fig. 2: Left: Demagnetization curves of granular SmCo thin films. Right: Second quadrant of the *BH*-loop of granular SmCo thin films. [a]external field is applied 45° the c-axes of the bicrystal structure (H||MgO[011]), [b]external field parallel or prependicular to c-axes the bicrystal structure (H||MgO[001]).

3. Epitaxial SmCo hard magnetic films

Demagnetization curves were calculated for (11$\bar{2}$0)-oriented SmCo and (1$\bar{1}$00)-oriented SmCo films. For the uniaxial structure, (1$\bar{1}$00)-oriented SmCo, the external field was applied parallel to the c-axis. For the bicrystal structure, (11$\bar{2}$0)-oriented SmCo, the demagnetization curves were calculated for two different angles of the external field. The angle between the field and the c-axes was either 45° (configuration a) or 0° and 90° (configuration b). The film thickness is 10 nm. Fig. 2 shows the demagnetization curves and the second quadrant of the *BH*-loop.

The uniaxial sample shows a perfectly square demagnetization curve with a coercivity of 19.8 MA/m. This is significantly higher than the values obtained experimentally [2,15]. This discrepancy might be due to structural defects that lower the magnetocrystalline anisotropy in the thin film as compared to the bulk value. Indeed magnet measurements [15] reveal an anisotropy constant of SmCo thin films which is about a factor of 4 smaller than the bulk value [19].

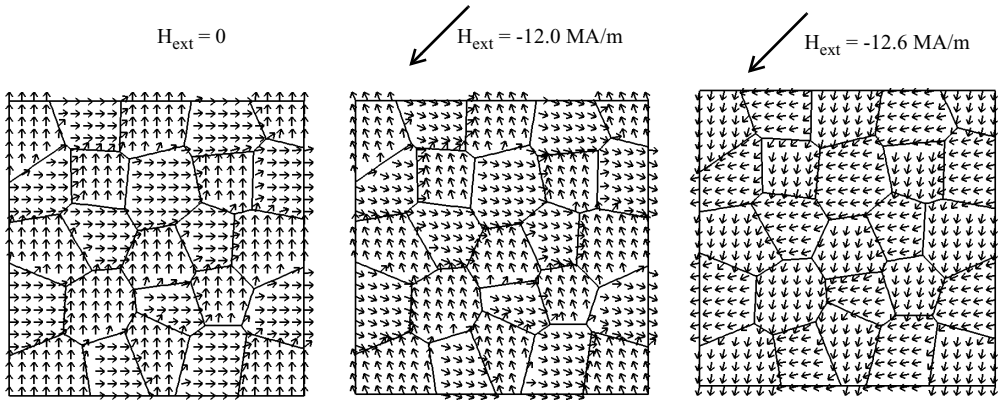

Fig. 3: Magnetization configuration during the reversal of a bicrystal SmCo film with the external field applied at 45° with respect to the c-axes.

The coercivity of the bicrystal sample depends on the orientation of the applied field with respect to the easy axes. If the field is applied at 45° the coercive field is higher than at a field angle of 0° or 90° degrees. This behavior corresponds well to experimental results [2] and has to be attributed to intergrain exchange interactions. Since the easy axes lie perpendicular to each other, strong exchange interactions between the grains lead to an effective easy direction being parallel to an intermediate orientation. Fig. 3 shows the remanent magnetic state of the bicrystal structure, the magnetic state just before magnetization reversal, and the magnetic state just after reversal. Under the influence of an inverse external field the magnetization rotates reversible out of the local c-axis. When the expense of anisotropy and exchange energy becomes too large the magnetization of the grains switches irreversibly. The energy density products are 60 kJ/m^3 and 127 kJ/m^3 for the bicrystal film with a field angle of 45° with respect to the c-axes and with field angles of 0°/90° with respect to the c-axes, respectively. The uniaxial film shows an energy density product of 232 kJ/m^3.

4. SmCo / Co bilayers

Fig. 4 shows the calculated demagnetization curves and corresponding *BH*-loop of 10 nm SmCo / 10 nm Co and of 10 nm SmCo / 5 nm Co. The shape of the demagnetization curves agrees well with experimental data [15] and has to be attributed to reversible rotations within the soft magnetic layer. Fig. 5 shows the gradually rotating magnetization structure within the soft layer and the hard layer. The magnetization configuration are plotted a different distances from the top surface of the soft layer. The reversible twist of the magnetization penetrates considerably into the hard layer. This agrees well with the results of recent experiments using spin-polarized neutron reflectometry [24] that clearly show the reversible magnetization in FePt/NiFe bilayers involves a portion of the hard ferromagnet.

At small inverse fields exchange interactions between the uniaxial SmCo film and the Co layer keep the Co moments parallel to the c-axes of the SmCo film. When the external field reaches the nucleation field, a magnetization twist is introduced into the soft layer which corresponds to the sharp drop of the magnetic polarization during reversal. If $|H_N|$ is too small the second quadrant of the *BH*-loop is no straight line but shows a knee at the nucleation field. For the 10 nm SmCo / 10 nm Co bilayer equation (2) is not fulfilled and $\mu_0|H_N| < J_s/2$. As a consequence the reversible rotations of the Co moments limit the energy density product. The $(BH)_{max}$ of 389 kJ/m^3 is slightly lower than the maximum possible value of 396 kJ/m^3. Perfect exchange hardening can be achieved if the Co layer thickness is reduced to 5 nm. The Co layer remains stable up to external field of

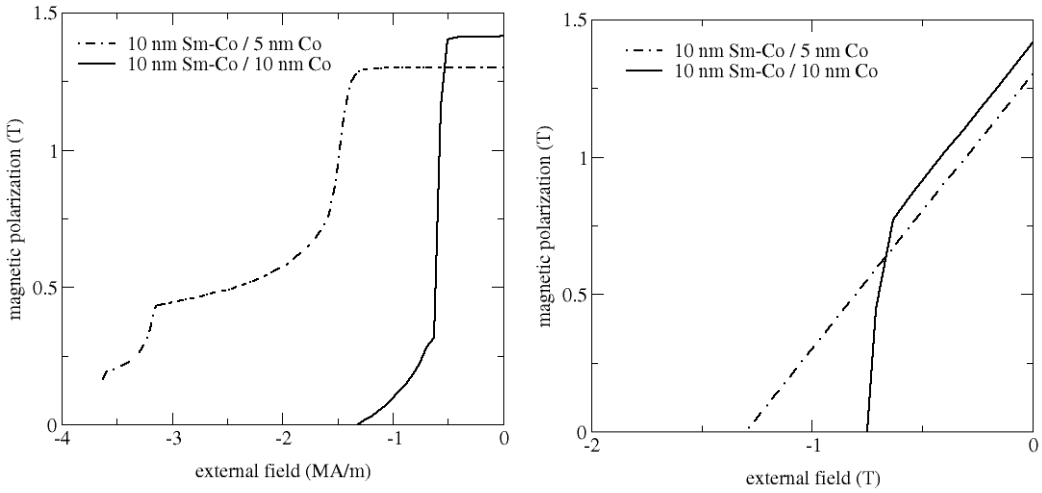

Fig. 4: Left: Demagnetization curves of SmCo/Co bilayers. Right: Second quadrant of the BH-loop of a SmCo/Co bilayers.

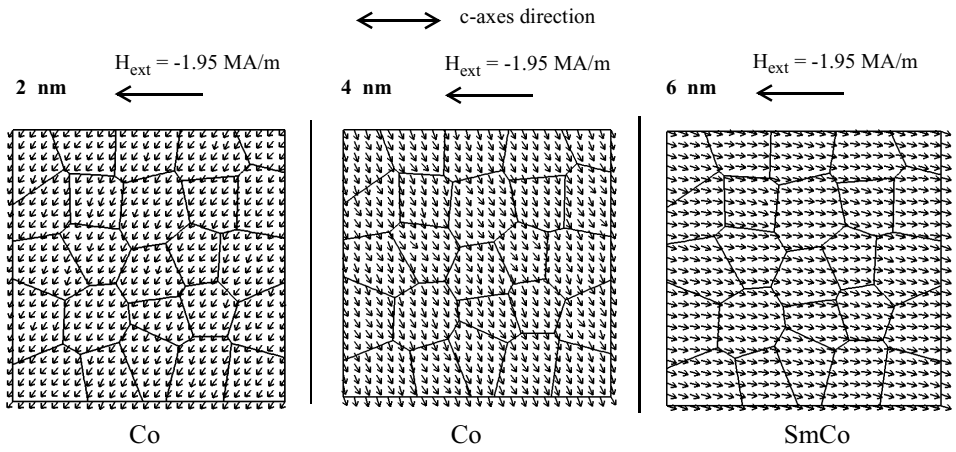

Fig. 5: Magnetization twist in a 10 nm SmCo / 5 nm Co bilayer. The plots give the magnetization configuration in a depth of 2 nm, 4 nm, and 6 nm from the top surface of the soft layer. The last slice (6 nm) is within the hard layer at a distance of 1 nm from the hard/soft interface. The reversible rotation of the magnetization penetrates into the hard layer.

$H_{ext} = -1.45$ MA/m. However, the reduced saturation polarization causes a reduction of the maximum energy density product to $(BH)_{max} = 339$ kJ/m^3. Nevertheless, the calculations show that a Co layer of 5 nm thickness is sufficient to increase the energy density product considerable with respect to the single layer uniaxial SmCo film.

5. SmCo / Fe bilayers

The highest energy density products are obtained in SmCo / Fe bilayers due to the high saturation polarization of α-Fe. Fig. 6 shows the calculated demagnetization curves and corresponding *BH*-curves for various layer thicknesses. For the 10 nm SmCo / 10 nm Fe bilayer the shape of the demagnetization curve shows the typical exchange spring behavior. The low nucleation field of $|H_N| = 0.49$ MA/m causes a steep decrease of the *BH*-loop which considerably reduces the energy density product with respect to its maximum possible value. Exchange hardening is more effective for thinner soft magnetic layers. The energy density product increases from 390 kJ/m^3 to 405 kJ/m^3

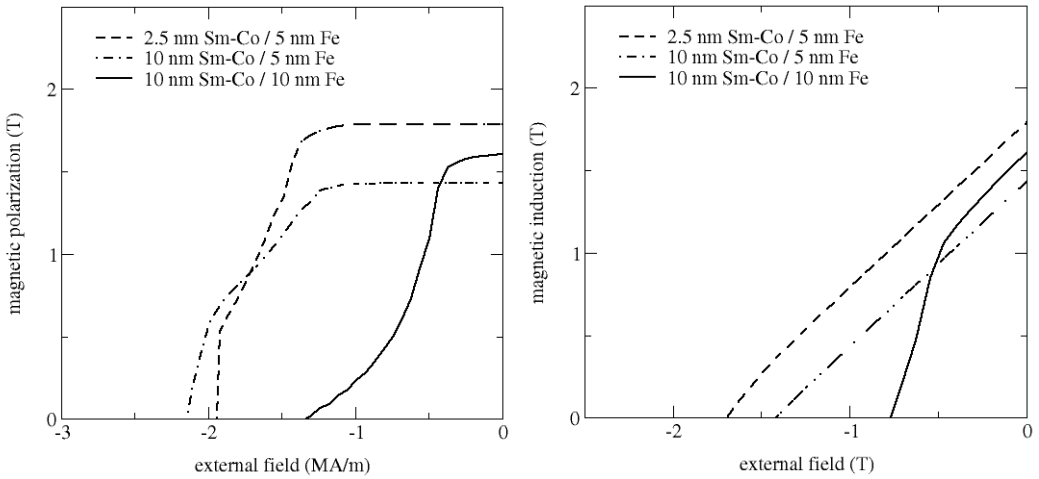

Fig. 6: Left: Demagnetization curves of SmCo/Fe bilayers. Right: Second quadrant of the BH-loop of a SmCo/Fe bilayers.

if the Fe layer thickness is decreased from 10 nm to 5 nm. A reduction of the hard layer thickness increases the volume fraction of the soft magnetic phase and in turn increases the saturation polarization, J_s. This will increase the energy density product as long as the system is stable at sufficiently large inverse fields. The energy density product reaches 644 kJ/m^3 for a 2.5 nm SmCo / 5 nm Fe bilayer. Fig. 7 shows the reversible rotation of the magnetization in a 10 nm SmCo / 10 nm Fe bilayer. Initially, the magnetization rotates in opposite directions in different regions of the film. With increasing rotation angle the exchange energy between the different regions become too large and the magnetization spontaneously switches within the smaller region to the twist direction of the large region and the soft magnetic moments become aligned almost parallel to each other. At this value of the external field the magnetization of the soft layer shows alread a substantial twist. Again reversible rotations penetrate substantially into the hard layer. Magnetization angles up to 30 degrees with respect to the easy axis are found in a depth of 1.5 nm

Pollman and co-workers [25] investigated the domain structure of a buried SmCo layer in SmCo/Fe spring magnet using X-ray magnetic circular dichroism. The magnetic images showed domain walls not oriented parallel the easy axis of magnetization but at angles between 45° and 90°. The micromagnetic simulations show that multi-domain states may form in the SmCo layer after an irreversible switching event. Fig. 8 shows the domain formation during irreversible switching of the hard layer of a 2.5 nm SmCo / 5 nm Fe bilayer. The right most image is a transient magnetic state obtained during the expansion of a reversed domain within the hard magnetic layer.

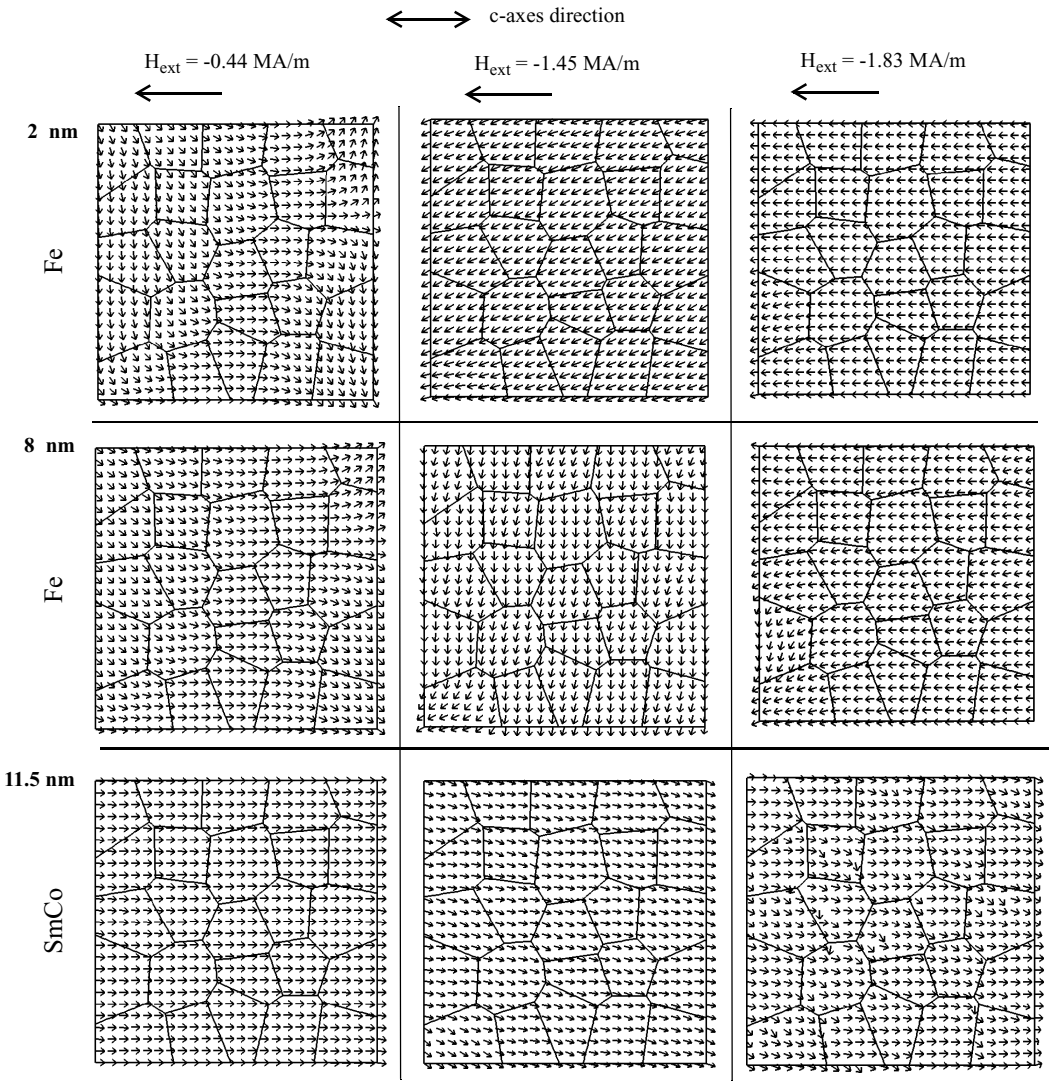

Fig. 7: Magnetization twist in a 10 nm SmCo / 10 nm Fe bilayer. The plots give the magnetization configuration in a depth of 2 nm, 8 nm, and 11.5 nm from the top surface of the soft layer. The last slice (11.5 nm) is within the hard layer at a distance of 1.5 nm from the hard/soft interface. From left to right the opposing field is increased.

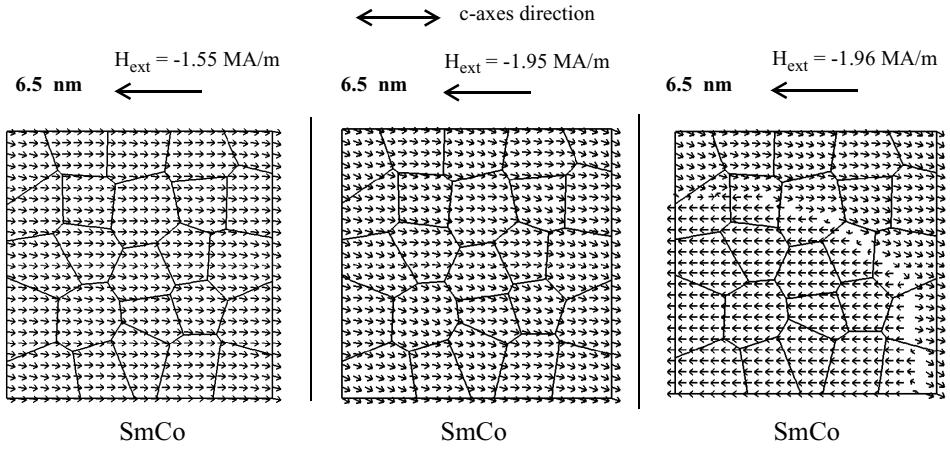

Fig. 8: Magnetization reversal in the hard layer of a 2.5 nm SmCo / 5 nm Fe bilayer. The plots give the magnetization configuration in a depth of 6.5 nm from the top surface of the soft layer. The slices are within the hard layer at a distance of 1.5 nm from the hard/soft interface. Irreversible switching occurs at $H_{ext} = -1.96$ MA/m.

6. Summary

Exchange hardening was investigated in SmCo exchange spring bilayers using finite element micromagnetic simulations. The basic results are summarized in Table 2. The calculations show that a high stability of the soft magnetic layer against magnetization reversal is required, in order to obtain the maximum possible energy density product. The critical field that introduces the twist into the soft layer, which in turn causes a sharp drop in the demagnetization curve, decreases considerable with decreasing thickness of the soft layer. A sufficiently large stability of the soft magnetic phase is obtained for soft layer thicknesses of about 5 nm. Since the domain wall width of SmCo is as low as 2.2 nm, a hard layer thickness of only 2.5 nm is enough to maintain exchange hardening. Energy density products up to 644 kJ/m^3 can be obtained in optimally structured SmCo/Fe bilayers. This value is considerably higher than the energy density product of high performance, sintered $Nd_2Fe_{14}B$ magnets.

Table 2: Magnetic properties of SmCo thin films and SmCo based exchange spring bilayers. t_{hard} and t_{soft} are the thicknesses of the hard and soft magnetic layers. J_{sat} and J_r are the saturation polarization and the remanent polarization. $H_{N,soft}$ and ${}_JH_c$ are the nucleation field of the soft layer and the coercive field. $(BH)_{max}$ is the energy density product.

	t_{hard} (nm)	t_{soft} (nm)	J_{sat} (T)	J_r (T)	$H_{N,soft}$ (MA/m)	${}_JH_c$ (MA/m)	$(BH)_{max}$ (kJ/m^3)
SmCo ($1\bar{1}00$)	10	-	1.07	1.07	-	19.8	232
SmCo ($11\bar{2}0$)[a]	10	-	1.07	0.8	-	12.2	127
SmCo ($11\bar{2}0$)[b]	10	-	1.07	0.55	-	7.7	60
SmCo / Co	10	10	1.42	1.41	0.56	1.3	389
SmCo / Co	10	5	1.3	1.3	1.45	3.6	339
SmCo / Fe	10	10	1.61	1.6	0.49	1.32	390
SmCo / Fe	10	5	1.43	1.43	1.42	2.14	405
SmCo / Fe	2.5	5	1.79	1.79	1.42	1.94	644

a. H || MgO[011]
b. H || MgO[001]

Acknowledgement

This work is supported by the Austrian Science Fund (Y-132 PHY).

7. References

[1] J. Barnes and P. Hut, “A hierarchical O(n log n) force calculation algorithm,” Nature, 324, pp. 446-449, 1986.

[2] M. Benaissa, K. M. Krishnan, E. E. Fullerton, J. S. Jiang, “Magnetic anisotropy and its microstructural origin in epitaxially grown SmCo thin films,” IEEE Trans. Magn., vol. 34, pp. 1204-1206, 1998.

[3] J. Bernardi, T.Schrefl, J. Fidler, T. Rijks, K.de Kort, V. Archambault, D. Pere, S. David, D. Givord, J.F. Sullivan, P. Smith, J.M.D. Coey, U. Czernik and M. Grönefeld, “Preparation, magnetic properties and microstructure of lean rare-earth permanent magnetic materials,” J. Magn. Magn. Mater., vol. 219, pp. 186-198 (2000).

[4] R. W. Chantrell, J. Fidler, T. Schrefl, M. Wongsam, “Micromagnetics: Finite Element Approach,” Encyclopedia of Materials: Science and Technology, Elsevier Science, 2001, pp. 5651-5661.

[5] H. J. Cho, S. Bhansali, C. H. Ahn, “Electroplated thick permanent magnet arrays with controlled direction of magnetization for MEMS application,” J. Appl. Phys., vol. 87, pp. 6340-6342, (2000).

[6] J. Fidler, T. Schrefl and D. Suess, “Grain boundaries in high performance magnets, reasons for poor or excellent properties,” Proc. of Workshop on Grain Boundaries: Their Characterisation and influence on properties, Birmingham, UK, Sept. 1999, edited by I.R. Harris and I.P. Jones, The University Press, Cambridge, 2001, pp. 147-163.

[7] R. Fischer, “ Fundamental magnetization processes in nanoscaled composite permanent magnets,” Phys. Rev. B., vol.57, pp.10723-10732, 1998.

[8] D. R. Fredkin, T. R. Koehler, “Hybrid method for computing demagnetizing fields,” IEEE Trans. Magn., vol. 26, pp. 415-417, 1990.

[9] H. Fukunaga and Nakamura, “Computer simulation of magnetic properties of anisotropic nanocomposite magnets,” IEEE Trans. Magn., vol. 36, pp. 3285-3287, 2000.

[10] E. E. Fullerton, J. S. Jiang and S. D. Bader, “Hard/soft magnetic heterostructures: model exchange-spring magnets,” J. Magn. Magn. Mater., vol. 200, pp. 392-404, 1999.

[11] E. Goto, N. Hayashi, T. Miyashita, K. Nakagawa, J. Appl. Phys., vol. 36, 2951, 1965.

[12] G. C. Hadjipanayis, W. Tang, Y. Zhang, S. T. Chui, J. F. Liu, C. Chen, and H. Kronmüller, “High temperature 2:17 magnets: Relationship of magnetic properties to microstructure and processing,” IEEE Trans. Magn., vol. 36, pp. 3382-3387, 2000.

[13] O. Hellwig, J. B. Kortrigh, K. Takano, E. E. Fullerton, “Switching behavior of Fe-Pt/Ni-Fe exchange-spring films studied by resonant soft-x-ray magneto-optical Kerr effect,” Phys. Rev. B, vol. 62, 11694-11698, 2000.

[14] S. Hirosawa, H. Kanekiyo, Y. Shigemoto, “Materials properties and utilization of $Fe_3B/Nd_2Fe_{14}B$-type nanocomposite permanent magnets based on Nd-Fe-Cr-Co-B,” in Advanced Hard and Soft Magnetic Materials. Symposium. Mater. Res. Soc, Warrendale, PA, USA, 1999, pp.141-152.

[15] J. S. Jiang, E. E. Fullerton, C. H. Sowers, A. Inomata, S. D. Bader, A. J. Shapiro, R. D. Shull, V. S. Gornakov, V. I. Nikitenko, “Spring magnet films,” IEEE Trans. Magn., vol. 35, pp. 3229-3234, 1999.

[16] J. W. Judy and N. Myung, “Magnetic Materials for MEMS”, Proceedings of the MRS Workshop on MEMS Materials, San Francisco, California, (April 5-6, 2002), pp. 23-26.

[17] E. F. Kneller and R. Hawig, “The exchange spring magnet: A new material principle for permanent magnets,” IEEE Trans. Magn., vol. 27, pp. 3588-3600, 1991.

[18] H. Kronmüller and D. Goll, “Micromagnetic theory of the pinning of domain walls at phase boundaries,” Physica B, vol. 319, pp. 122-126, 2002.

[19] E. Lectard, C. H. Allibert and R. Ballou, “Saturation magnetization and anisotropy fields in the $Sm(Co_{1-x}Cu_x)_5$,” J. Appl. Phys., vol. 75, pp. 6277-6279, 1994.

[20] J. C. Mallinson, “On damped gyromagnetic precession,” IEEE Trans. Magn., vol. 23, pp. 2003-2004, 1997.

[21] K. Mibu, T. Nagahama, T. Shinjo and T. Ono, “Magnetoresistance of quasi-Bloch-wall induced in NiFe/CoSm exchange-spring bilayers,” J. Magn. Magn. Mater., vol. 177-181, pp. 1267-1268, 1998.

[22] T. Nagahama, K. Mibu and T. Shinjo, “The magnetization process and magnetoresistance of exchange-spring bilayer systems,” J. Phys. D: Appl. Phys., vol. 31, pp. 43-49, 1998.

[23] J. Nogués and Ivan K. Schuller, “Exchange bias,” J. Magn. Magn. Mater., vol. 192, pp. 203-232, 1999.

[24] K. V. O’Donovan, J. A. Borchers, C. F. Majkrzak, O. Hellwig, E. E. Fullerton, “Pinpointing chiral structures with front-back polarized neutron reflectometry,” Phys. Rev. Lett., vol. 88, pp. 67201-67204, 2002.

[25] J. Pollmann, G Srajer, D. Hakel, J. C. Lang, J. Maser, J. S. Jiang, S. D. Bader, “Magnetic imaging of a buried SmCo layer in a spring magnet,” J. Appl. Phys., vol. 89, pp. 7165-7167, 2001.

[26] T. Schrefl and J. Fidler, “Numerical simulation of magnetization reversal in hard magnetic materials using a fintie element method,” J. Magn. Magn. Mater., vol. 111, pp. 105-114, 1992.

[27] T. Schrefl, “Finite elements in numerical micromagnetics part I: granular hard magnets,” J. Magn. Magn. Mater., vol. 207, pp. 45-65, 1999.

[28] R. Skomski, J. M. D. Coey, “Giant energy product in nanostructured two-phase magnets,” Phys. Rev. B, vol. 48, pp. 15812-15816, 1993.

[29] R. Skomski, J. M. D. Coey, “Permanent magnetism,” Bristol, UK , Philadelphia, PA : Institute of Physics Pub., 1999.

[30] D. Suess, V. Tsiantos, T. Schrefl, J. Fidler, W. Scholz, H. Forster, R. Dittrich and J. J. Miles, “Time resolved micromagnetics using a preconditioned time integration method,” J. Magn. Magn. Mater., in press, 2002.

[31] Y. Q. Wu, D. H. Ping, B. S. Murty, H. Kanekiyo, S. Hirosawa, K. Hono, “Influence of heating rate on the microstructure and magnetic properties of $Fe_3B/Nd_2Fe_{14}B$ nanocomposite magnets,” Scripta. Mater., vol. 45, pp. 355-362 (2001).

[32] W. Yang, D. N. Lambeth, and D. E. Laughlin, “Dependence of Co anisotropy constants on temperature, processing, and underlayer,” J. Appl. Phys., vol. 87, pp. 6884-6886, 2000.